Umbilical defect dynamics in an inhomogeneous nematic liquid crystal layer

Valeska Zambra,[1,*] Marcel G. Clerc,[1,†] Raouf Barboza,[1,2,‡] Umberto Bortolozzo,[3,§] and Stefania Residori[4,3,‖]

[1]*Departamento de Física and Millennium Institute for Research in Optics, Facultad de Ciencias Físicas y Matemáticas, Universidad de Chile, Casilla 487–3, Santiago, Chile*

[2]*Dipartimento di Fisica, Università di Napoli Federico II, Complesso Universitario di Monte Sant'Angelo, Via Cintia, 80126 Napoli, Italy*

[3]*HOASYS, 1047 route des Dolines, 06560 Valbonne, France*

[4]*Institut de Physique de Nice, UMR7010, Université de Nice-Sophia Antipolis, CNRS, 1361 Route des Lucioles, 06560 Valbonne, France*

(Received 4 February 2020; accepted 22 May 2020; published 19 June 2020)

Electrically driven nematic liquid crystals layers are ideal contexts for studying the interactions of local topological defects, *umbilical defects*. In homogeneous samples the number of defects is expected to decrease inversely proportional to time as a result of defect-pair interaction law, so-called coarsening process. Experimentally, we characterize the coarsening dynamics in samples containing glass beads as spacers and show that the inclusion of such imperfections changes the exponent of the coarsening law. Moreover, we demonstrate that beads that are slightly deformed alter the surrounding molecular distribution and attract vortices of both topological charges, thus, presenting a mainly quadrupolar behavior. Theoretically, based on a model of vortices diluted in a dipolar medium, a $\frac{2}{3}$ exponent is inferred, which is consistent with the experimental observations.

DOI: 10.1103/PhysRevE.101.062704

I. INTRODUCTION

Irregularities in nature are one of the primary resources of the diversity of forms [1–6]. A paradigmatic example of these are fingerprints, which allow us to uniquely identify human beings. From a physical point of view, these correspond to the local or global loss of translation or rotation symmetry. Irregularities are commonly denominated defects. Depending on the geometrical shape of these irregularities they can be classified as localized or extended. Classical examples of localized and extended defects in condensed matter are dislocations and grain boundaries [7]. Defects are a consequence of the fact that systems out of equilibrium present the coexistence of spatially extended states [2–6]. Hence, irregularities connect different states. Among others, defects in rotationally invariant two-dimensional systems, i.e., vortices, attract a great deal of attention of the scientific community because of their universal character and intriguing topological properties [8]. These defects correspond to the local confluence of different orientational domains. Vortices have been observed in different physical contexts such as fluids, superfluids, superconductors, liquid crystals, fluidized anisotropic granular matter, magnetic media, optical dielectrics, and cosmology, to mention a few [8]. Mathematically, these solutions occur in complex fields and can be identified as pointlike singularities which locally break rotational symmetry. At a singular point, the amplitude of the order parameter is zero due to its single valuedness, and its phase changes continuously by an integer multiple of 2π around the singularity. The winding number, *topological charge*, is assigned by counting the number of phase jump around the phase singularity [8]. While the sign of the winding number is given by the sense of increment (positive) or decrement (negative) of phase jump [8]. As a convention, it is attributed to the positive (negative) value of the topological charge for the clockwise (anticlockwise) of the phase distribution. Indeed, vortices are topological defects since these solutions are created or destroyed by pairs with their respective opposite charge. Also, vortices can be induced by an external topological forcing [9–11].

Nematic liquid crystals are a soft matter material made of anisotropic rodlike shaped organic molecules [12–14], which results in strongly anisotropy media. In the nematic phase, the configuration of lowest energy is reached when all the rodlike molecules are on average aligned along one privileged direction. This privileged direction is usually imposed by the anchoring conditions of the recipient containing the liquid crystal [12–14]. Under the effect of sufficiently large external electric or magnetic fields, the molecules can be reoriented along or orthogonal to the direction of the applied field in order to minimize the free energy [15]. This reorientation generates the emergence of different domains and defects that separate them. In particular, nematic liquid crystal cells with negative anisotropic dielectric constant and homeotropic anchoring are a natural physical context where dissipative vortices and line defects can be observed and analyzed [12–14]. In this physical configuration, the dissipative vortices are usually called umbilical defects [16]. Due to the fact that these defects break the orientational order and by analogy with disclinations in crystals of condensed matter, Frank called these defects *disclination lines* [13,19]. These defects have accompanied liquid crystals since their discovery in 1889 by Lehmann [17] who called these intriguing localized structures as *kernels*. Likewise, they were observed in

*valesk.za@gmail.com
†marcel@dfi.uchile.cl
‡raouf.barboza@tut.fi
§umberto.bortolozzo@hoasys.fr
‖stefania.residori@hoasys.fr

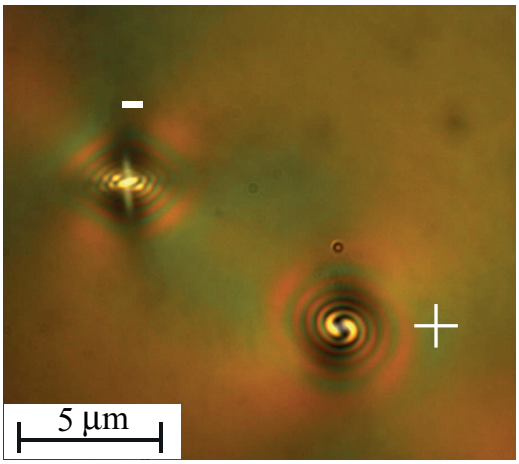

FIG. 1. Snapshot of umbilical defects of opposite charges observed in a nematic liquid crystal layer within circular crossed polarizers (CCP). Umbilical defect of positive (negative) charge has circular (square) shape.

a similar experimental setup by Friedel, who denominated these defects as *noyaux* [18]. Frank calculated the detailed structure of these defects based on the elasticity of nematic liquid crystals [19]. Despite the different designations given to the observed vortices in this physical framework, none of them were adopted by the liquid crystals community. There, the most widely used names are *nematic umbilical defects* and *disclination lines*. Henceforth, we will use the term umbilical defects, even though it is intended that these two names can be used indifferently.

The term umbilic defects was coined by Rapini [16] and refers to the structure of the defect which corresponds to a stringlike object in three dimensions. Umbilical defects in nematic liquid crystal layers have long been studied (see textbooks [12–14] and reference therein). Two types of stable defects with opposite charges are observed, which are characterized by being attracted to (repelled by) the opposite (identical) charge. Figure 1 shows the typical umbilical defects observed in the microscope using circular crossed polarizers. Note that such defects observed in liquid crystals are structurally similar to those found in magnetic systems, superfluids, superconductors, and Bose-Einstein condensates. However, umbilical defects are dissipative states, that is, they exhibit an entirely different dynamical evolution due to the strongly dissipative nature of liquid crystals.

Due to the complexity of the elastic theory of liquid crystals, the analytical study of the umbilical defects is inaccessible [12,13]. Weak nonlinear analysis, valid close to the orientational instability of the molecules, allows describing the dynamics of a nematic liquid crystal layer by the Ginzburg-Landau equation with real coefficients [10,11,20–23]. This amplitude equation has gathered a great interest by describing several physical systems such as fluids, superfluids, superconductors, liquid crystals, magnetic media, and optical cavities, to mention a few (see the textbook [8] and reference therein). Indeed, this amplitude equation describes the onset of a degenerate stationary instability with rotational invariance [4] or a stripe pattern instability in anisotropic systems [5,24]. Hence, the dynamics described by this model is common to a wide class of physical systems. The Ginzburg-Landau equation with real coefficients allows understanding the emergence of different orientational domains, two types of stable vortices with a positive and negative charge and their respective dynamics. In this approach, both local defects are indistinguishable in their amplitude magnitude. As a result of the phase invariance of this amplitude equation, they account for a continuous family of solutions, characterized by a phase parameter [8]. Besides, one can characterize analytically the vortex-pair interaction [8], which is in agreement with experimental evidence [22].

In a first approximation, the vortex-pair interaction is described by an overdamping system with force proportional to the inverse of their distance [12,25]. Experimental observations provide asymptotically agreement with this approach [26–29]. In general, the law of the number of defects as a function of time can be derived based on defect-pair interaction law and self-similarity statements [30,31]. The resulting self-similar behavior is well known as a *coarsening* process, in analogy with domain growth in metallic alloy phase separations [32] and in foam drainage [33]. Using the vortices' interaction law, one can show that the number of defects in homogeneous nematic samples decreases inversely proportional to time, which has been previously observed [26,29,34]. Likewise, using phase XY model, one obtains the same decay law for the vortices' number [29].

To study the coarsening dynamics in inhomogeneous nematic samples, we use cells in which the thickness of the liquid crystal layer is fixed by monodispersed glass microspheres spread randomly inside the sample. By characterizing the creation and interaction process of umbilical defects, we show that the presence of the beads alters the coarsening law. Indeed, even though most of the glass beads do not affect the vortices' dynamics, those that are more geometrically deformed attract vortices of both topological charges, presenting mainly a quadrupolar behavior, an interaction weaker than the usual interaction between dipolar vortices. This effect actively modifies the collective behavior of the vortex system and alters the scaling law [35]. Depending on the different disordered configurations of beads, the system exhibits different statistical temporal evolutions of the number of defects, exhibiting power laws with different exponents. Theoretically, based on a model of vortices diluted in a dipolar medium and self-similarity, a coarsening law with exponent $\frac{2}{3}$ is inferred. This critical exponent shows a good agreement with the experimental observations.

II. EXPERIMENTAL SETUP

To study the dynamics of umbilical defects, we consider two different types of liquid crystal cells with approximately the same thickness. The first cell, *homogeneous sample*, is made of two indium tin oxide (ITO, transparent conductor) coated glass slabs. The glass slabs are treated on the ITO side to promote orthogonal alignment of the liquid crystal molecules; this alignment is termed as homeotropic anchoring [12–14]. The glass slabs are held together with a thin sheet of polymer spacers such that, the treated faces form a gap in which the liquid crystal is, then, infiltrated.

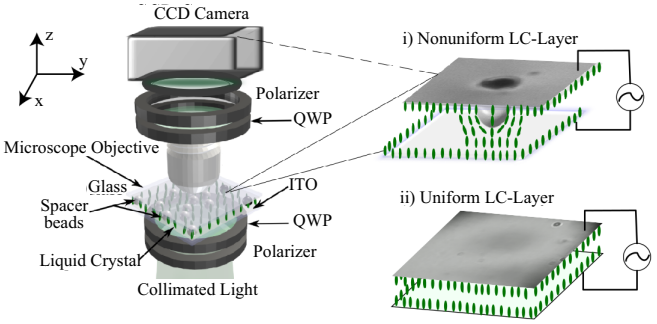

FIG. 2. Schematic representation of the experimental setup of a nematic liquid crystal layer with negative dielectric constant and homeotropic anchoring under the influence of a vertical voltage. The essential parts of the setup are emphasized. Crossed polarizers, either linear or circular, are used in order to analyze the liquid crystal texture. Two types of liquid crystal cells have been studied: (i) homogeneous and (ii) inhomogeneous (with glass beads) sample.

The spacers fix the thickness of the gap, which is about 15 μm thin. The second cell, *inhomogeneous sample*, from Instec Inc. (SB100A150uT180 liquid crystal cell), also has a homeotropic alignment. The spacing gap is achieved by sputtering spacer beads made of microsphere clear and transparent ceramics or glass onto the cell substrate before assembly [36]. The diameter of the microspheres fixes the cell gap, which is about 15 μm for the chosen cell. Both cells were filled by capillarity with MLC-6608 nematic liquid crystal (from Merck), characterized by a negative dielectric anisotropy. Figure 2 depicts the experimental setup. To achieve maximum contrast, resolution, a collimated white light (Köhler type illumination) from a microscope condenser is sent onto the liquid crystal cell, the latter mounted on a translation stage. The texture of the liquid crystal is imaged on a CCD camera through a microscope objective and relay lenses.

From here on, we will denote by $\hat{z}$ the normal to the glass plates. Due to inherent elastic forces between the molecules, in a certain temperature range, the absence of external stimulus, to minimize the elastic free energy, the alignment in the bulk of the liquid crystal layer will be uniform, thus parallel to the $\hat{z}$ direction in order to accommodate that of the boundaries. Both cells are biased with a low-frequency sinusoidal voltage ($\approx$100 Hz) and are operated at room temperature where the liquid crystal is in the nematic phase. The resulting electric torque will tend to rotate the molecules away from the z axis. Over a critical threshold voltage, called Fréedericksz transition voltage [12–15], the molecules tilt away from their vertical position. Due to the 2π azimuthal degeneracy in possible directions of orientation, different domains, and umbilical defects will be generated in the nematic liquid crystal layer where the orientation can not be topologically smoothed out [12–14,16–19].

The cells contain liquid crystals that are intrinsically birefringent in the nematic phase. Two crossed polarizers, the first to polarize the illumination source and the second to analyze the polarization of the light exiting the cell, are used to recover the averaged two-dimensional texture of the liquid crystal layer, where the average is along $\hat{z}$. Indeed, with a good approximation, the cell can be considered as a two-dimensional (2D) uniaxial birefringent material with varying optical axis aligned in the xy plane at an angle $\theta(x, y)$ with the x axis and providing a phase retardation $\delta(x, y) = 2\pi L(\tilde{n}_e - n_o)/\lambda$. Here, L represents the thickness of the liquid crystal layer, λ the operating wavelength of the illumination source, and $\{n_o, \tilde{n}_e\}$ the ordinary and, respectively, extraordinary refractive index averaged over the longitudinal coordinate. The optical axis can be viewed as the averaged azimuthal direction of the molecules in the xy plane or, equivalently, their projection onto the xy plane. The averaged extraordinary index $\tilde{n}_e$ is related to n_0, n_e (the extraordinary refractive index of fields polarized along the optical axis) and the tilt ψ of the molecules with respect to the z axis by [12,14]

$$\tilde{n}_e = \int_0^L \frac{n_e n_o}{\sqrt{n_e^2 \cos^2\psi + n_o^2 \sin^2\psi}} dz. \tag{1}$$

To probe the evolution of the texture of the liquid crystalline layer, hence, the dynamics of the defects, we rely on polarizing optical microscopy techniques based on crossed linear polarizers (CLP). By using Jones matrix formalism [37], the intensity is given by [37]

$$I_{\mathrm{CLP}}(x, y) = I_0 \sin^2 \frac{\delta(x, y)}{2} \sin^2 2\theta(x, y), \tag{2}$$

where I_0 is the maximum input intensity. Likewise, the crossed circular polarizer (CCP) configuration is achieved when two quarter wave plates are inserted in the previous configuration, with the first wave plate at $\pm 45^\circ$ with respect to the axis of the input polarizer, and the fast axis of the second wave plate orthogonal to the first one. In this case, the intensity after the cell depends as follow on the phase retardation [37]

$$I_{\mathrm{CCP}}(x, y) = I_0 \sin^2 \frac{\delta(x, y)}{2}. \tag{3}$$

In the experiment both imaging configurations, either CLP or CCP, are used with the polarizing microscope, depending on the defect features that we want to emphasize, either position or charge.

In the Ginzburg-Landau theoretical framework, positive and negative defects are indistinguishable, that is, they are supposed to look the same for CLP and CCP. However, due to the anisotropy of the elastic constants of liquid crystals, they can be distinguished under appropriate conditions. Figure 1 shows two umbilics, one with positive and the other with negative charge. The micrograph is taken with crossed circular polarizers. Note that the defect with positive charge has a circular shape, while the negatively charged umbilic has a square shape [38]. These geometrical features allow us to distinguish the sign of the topological charges. Note that these geometric features persist under linear crossed polarizers [38].

III. RESULTS AND DISCUSSIONS

First, in order to figure out the coarsening dynamics of the vortices in a homogeneous cell, we proceed as follows: we start with establishing the vortex-pair interaction law and, then, by using its self-similarity properties, we deduce the coarsening law.

A. Vortex-pair interaction law

Based on the Ginzburg-Landau equation with real coefficients that describes liquid crystal dissipative dynamics, the fine analysis of the vortex interaction law is a daunting task due to the logarithmic divergence of the energy associated with each vortex and the vortex-pair interaction with the size of the system [8,12]. In the case of finite size systems, the vortex-pair interaction law can be approximated for long distances by [8]

$$M\dot{\mathbf{r}} = \frac{q}{||\mathbf{r}||}\hat{r}, \tag{4}$$

where $\mathbf{r}(\mathbf{t})$ is the vector that joins the positions between vortices, $||\mathbf{r}||$ is the magnitude of the vector $\mathbf{r}$, $\hat{r} \equiv \mathbf{r}/||\mathbf{r}||$ is a unitary vector, q is the product of the topological charges of interacting vortices ($q = \pm 1$), then it is positive (negative) when both vortices have the same (different) charge, and M stands for the vortex mobility which depends on the size of the system, the properties of the liquid crystal, and the applied voltage. When one considers the effect of the phase of one vortex on the other, mobility depends logarithmically in $\dot{r}$ [5]. However, this correction is weak [22] and can be neglected when fine interaction between defects is not of concern and only collective effects are of interest. Thus, the constant mobility approximation is appropriate in the interpretation of the experimental results [39]. Hence, the interaction between vortices is equivalent to overdamped particles with a force inversely proportional to their distance. Note that when the vortex distance is small, of the order of the vortex core, the previous model for dynamics is no longer valid. In this case, vortices of opposite charge merge and disappear together.

In brief, the dynamics of interaction between vortices tend to homogenize the deformations of molecular orientation in order to minimize the free energy of the system. As we have mentioned, experimental characterization of the vortex-pair interaction provides a fair agreement with the previous results [22,26,28,29].

B. Theoretical derivation of the coarsening law for a diluted gas of vortices

In the context of dilute gases of n vortices in a homogeneous medium, the interaction between defects is governed by

$$M\dot{\mathbf{r}}_i = \sum_{j\neq i}^{n} \frac{q_{ij}}{r_{ij}}\hat{r}_{ij}, \qquad i = \{1, 2, \ldots, n\} \tag{5}$$

where $r_{ij} \equiv ||\mathbf{r}_i - \mathbf{r}_j||$ is the distance between the ith and jth vortex, $\hat{r}_{ij}$ in the unitary vector directed from jth to ith vortex, and q_{ij} is the, respective, product of the topological charges of vortices. Hence, the dynamics of a gas of n vortices corresponds to an overdamped n-body problem. Note that the above set of equations is invariant under the self-similarity transformation

$$\begin{aligned} \mathbf{r}_i &\to \lambda \mathbf{r}_i, \\ t &\to \lambda^2 t. \end{aligned} \tag{6}$$

If one dilates or expands time and space, using the above scaling, then, the set of Eqs. (5) are invariant. We can introduce $N(t)$, the number of vortices at time t, which can be estimated as

$$N(t) = \frac{A}{\langle r\rangle^2}, \tag{7}$$

where A is the area of the sample under study, and $\langle r\rangle$ is the average distance between vortices. Because the set of Eqs. (5) governs the vortices dynamics, the average distance $\langle r\rangle$ and $N(t)$ are determined by the vortices' evolution. Then, $\langle r\rangle$ and $N(t)$ should also be self-similar with transformation (6). Hence, $N(\lambda^2 t) = A/\lambda^2\langle r\rangle^2$. From the previous equality, one infers that the only possibility is that the number of vortices scales as

$$N(t) = \frac{\beta}{t}, \tag{8}$$

with β a dimensional constant. Indeed, the number of defects decreases inversely proportional to time, so-called *coarsening law*. Experimentally, this law was, indeed, observed and validated in nematic liquid crystal samples [29,34].

C. Vortex creation and annihilation in a homogeneous liquid crystal cell: Experimental observations

To investigate the creation and annihilation process of vortices, we have conducted several experimental analyses on the vortex gas dynamics. We apply a large enough voltage to the liquid crystal layer in-between crossed polarizers, which spontaneously generates hundreds of umbilical defects in random positions as a result of thermal fluctuations and inherent inhomogeneities in the system. Initially, the emergence of vortices is preceded by the appearance of domain walls [cf. Fig. 3(b)], which are created by thermal fluctuations. These domain walls are unstable, generating the emergence of topological defects of charges $\pm\frac{1}{2}$, which move along the domain walls. These topological defects are characterized by the joint of two black brushes [39]. Figure 3(c) illustrates the different observed local and global defects. These defects with half topological charge are characterized by the joint of two arms and a domain wall. Collisions of these defects with the same topological charge generate umbilical defects and with different charges cancel each other out. After this rapid transient, a dilute vortex gas is established in the system [cf. Fig. 3(d)]. Thanks to the crossed linear polarizers, the position of the umbilical defects is recognized by the interception of four black curves [12]. Subsequently, the defects exhibit a dynamic of attraction and repulsion following the interaction law (5). Figure 3 shows a temporal sequence of snapshots, which emphasize the natural evolution of the defect gas. From the temporal sequences and through an appropriate recognition software (open source Java image processing program Fiji), we can determine the number of vortices and their respective positions. Thus, we acquire the evolution of the number of vortices $N(t)$ as a function of time. Figure 3(f) summarizes the temporal evolution of $N(t)$ starting from the switch-on of the driving voltage V_0. From this temporal evolution, one can separate the process in two stages: one associated with the creation of vortices, *growth stage*, and, later, a second regime characterized by the process of decay of the number of vortices, *coarsening stage*.

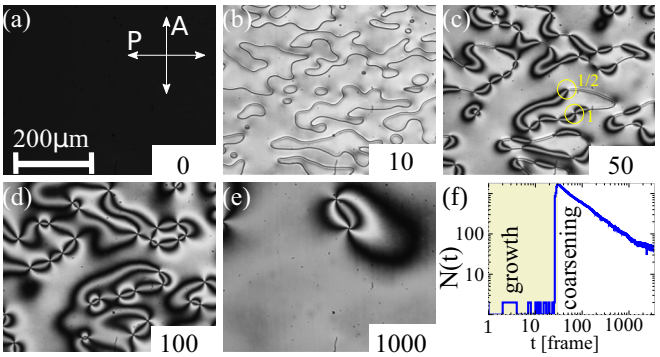

FIG. 3. Creation and annihilation dynamics of umbilical defects in a homogeneous nematic liquid crystal layer under two crossed linear polarizers. The temporal sequence of snapshots from left to right and top to bottom (a)–(e) corresponds to driving the cell from zero voltage to a voltage V_0 beyond the Fréedericksz transition threshold. The bottom numbers in each panel account for the respective frame. The temporal increment of each frame corresponds to 400 μs. The interception of four black brushes gives the position of umbilical defects with topological charge ± 1. (a) Liquid crystal cell without applied voltage, showing the orientation, respectively, of the polarizer (P) and analyzer (A). (b) Emergence of orientational domains after 800 μs the voltage is switched to $V_0 = 15\ V_{\rm rms}$. (c) Creation of vortices through reorganization of domains; circumferences and respective numbers account for the different topological charge of the defects. The interception of two black brushes gives the position of the defects with topological charge $\pm\frac{1}{2}$. (d) Diluted gas of vortices. (e) Vortex pair and (f) temporal evolution of the number of vortices $N(t)$.

D. Experimental determination of the coarsenin lawg in homogeneous cells

Based on the Ginzburg-Landau model, one expects the number of defects to decay with a power law. Figure 4 depicts the typical evolution of the number of umbilical defects as a function of time for a nematic liquid crystal layer driven to $V_0 = 70$ V with a frequency of 100 Hz. To compute and monitor the number of vortices in given time we have used an image processing package. From this plot, one infers that the

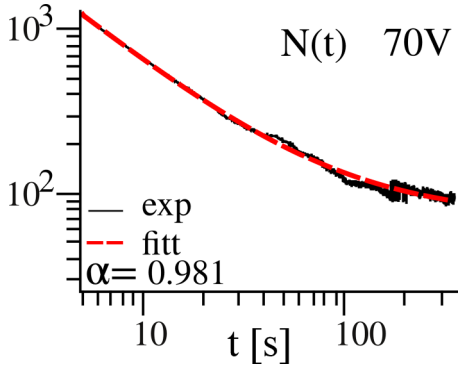

FIG. 4. Coarsening dynamics in a homogeneous cell. Number of umbilical defects as a function of time. The solid black and dashed curves are, respectively, the experimental evolution of $N(t)$ and the fitting curve $N_f(t) = \beta t^{-\alpha} + N_\infty$ with $\alpha = 0.981 \pm 0.001$, $\beta = 5.7 \times 10^3 \pm 2 \times 10^2$, and $N_\infty = 70 \pm 2$.

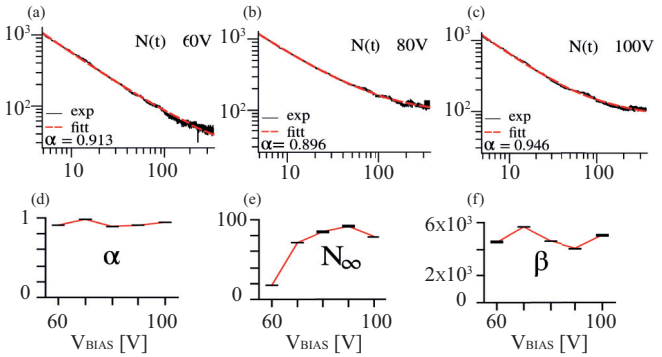

FIG. 5. Number of umbilical defects as a function of time. Coarsening process of umbilical defects in a homogeneous cell with different driven voltages (a) $V_0 = 60$ V, (b) $V_0 = 80$ V, (d) $V_0 = 100$ V, using the same frequency 100 Hz. The black and red curves account for the experimental data and fitting curve formula (9), respectively. Critical fitting exponent α (d), asymptotic number of vortices N_∞ (d), and β (e) as function of applied voltage.

number of vortices decays as a function of time with a power law. To determine the exponent of this coarsening process, we have considered the following fitting function:

$$N_f(t) = \beta t^{-\alpha} + N_\infty, \tag{9}$$

where $\{\beta, \alpha, N_\infty\}$ are fitting parameters, which account for the features of the liquid crystal and the cell under study. N_∞ stands for the imperfections of the system, which causes the vortices to become trapped in given positions, and the inaccuracy of the recognition method. Experimentally, we found that in the homogeneous samples under study the exponent $\alpha = 0.981$ provides a quite good agreement with the simplified description (5). Hence, this type of particle-type approach to the vortex dynamics in a homogeneous liquid crystal layer, ignoring the process of collision and nonlinear effect of mobility, gives a fair description of the average evolution of the vortices.

To study carefully the coarsening process, we have conducted a series of experiments with different voltages and the same frequency (100 Hz). Similar behaviors for the evolution of the vortex number are observed. Figure 5 summarizes the coarsening process for different voltages. From this analysis, we conclude that for different voltages the system exhibits a coarsening behavior. In particular, the critical exponent is close to $\alpha \sim 1$, which is consistent with the theory of the Ginzburg-Landau amplitude equation with real coefficients. Hence, this simplified theory of liquid crystal dynamics [21,23] appropriately accounts for the process of coarsening in a homogeneous nematic liquid crystal sample. In the next section, we will analyze the effect of inhomogeneities in the coarsening dynamics by using the inclusion of glass beads in the sample.

E. Experimental determination of the coarsening law in inhomogeneous liquid crystal cells

To investigate the interaction of the umbilics in the presence of randomly distributed inclusions in disordered liquid crystal media, we have conducted several experimental

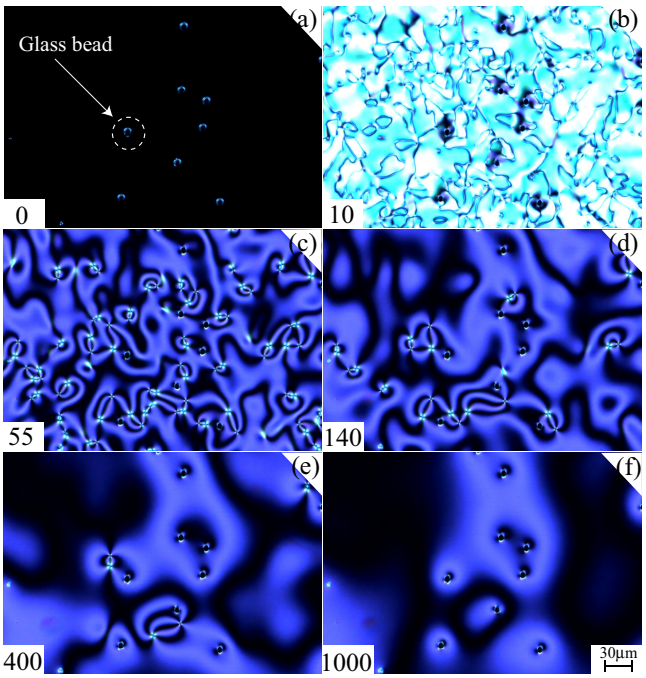

FIG. 6. Umbilical defect annihilation dynamics in an inhomogeneous liquid crystal cell with glass beads and in-between two linear crossed polarizers. Temporal sequence of snapshots from left to right and top to bottom depicts the vortex evolution starting from the switch-on of the driving voltage. The temporal increment of each frame corresponds to 0.33 s. The position of the umbilical defects is given by the interception of four black brushes. The white dashed circumference accounts for the position of a glass bead.

analyses of the vortex gas dynamics in a liquid crystal sample with glass beads. The inhomogeneous cell is observed in-between two crossed polarizers and by applying a large enough, beyond the Fréedericksz threshold, voltage. The glass beads are microspheres with a monodisperse distribution and a size of 15 μm. Figure 6(a) shows the liquid crystal cell without having an applied voltage. Because the anchoring is of the homeotropic type, under crossed polarizers the sample should appear as completely dark. However, the presence of glass beads distorts the configuration of the molecules in their surroundings. Hence, glass beads are detected by this molecular deformation reorientation, which changes the light polarization locally around each glass bead [see Fig. 6(a)]. As we mentioned earlier, the beads are randomly distributed. When a voltage is applied, initially, the emergence of domains is observed [see Fig. 6(b)], but now the process is affected by the presence of glass beads [35]. Later, the system is accompanied by the emergence of a gas of umbilical defects, as it is depicted in Fig. 6(c). Subsequently, the defect interaction dominates the dynamics, which is characterized by the constant decrease in the number of defects. Figure 6 shows a temporal sequence of snapshots depicting the vortex interaction in the cell. The natural question that emerges is, therefore, whether the coarsening dynamics is persistent under the inclusion of inhomogeneities in random positions.

To answer this question, we analyze the images with the particle tracking process, which allows us to determine the number of vortices and their respective positions. Figures 7(c) and 7(f) show the temporal evolution of the number of umbilical defects as a function of time for different zones of the liquid crystal sample. Each zone has an area of 1.43 mm^2 (cf. Fig. 7). In both graphs, we observe that the system exhibits a coarsening process with a power law, however, with different exponents. These power laws are obtained by realizing several experimental realizations (10 repetitions were performed for each parameter to obtain the characteristic exponents). Hence, the observed coarsening dynamics can be considered as a persistent phenomenon [35]. Nevertheless, depending on the distribution of the glass beads, we observe different power laws (cf. Fig. 7). Notice that the exponent deviates from the exponent determined by the law derived from the theory of the Ginzburg-Landau model for a homogeneous medium. Therefore, we can conclude that the presence, density, and distribution of glass beads affect the coarsening dynamics. The main effect, as we will see later, is produced by a small amount of deformed beads that interact and attract vortices.

TABLE I. Results of the measured bead density, computed fitting exponents, and entropy over an area of approximately 1.394 mm^2 on different observation zones.

Zone	**Density** (mm^2)	α	β	N_∞	**Entropy**
I	13.630	0.60	604.2	12.85	0.0210
II	17.217	0.88	1782.0	20.33	0.0136
III	20.803	0.25	246.4	22.44	0.00767
IV	21.521	0.71	1285.0	17.87	0.0091
V	23.673	0.70	1404.0	25.74	0.00772
VI	27.977	0.82	162.7	18.09	0.0057

To characterize the clustering and distribution of the glass beads, we have computed the Voronoi tessellation [40] of the glass beads in different observed zones [cf. Figs. 7(a) and 7(d)]. The respective histogram of the bead mutual distance is also computed on each observation zone [cf. Figs. 7(b) and 7(e)]. From these diagrams, we can measure the density of the beads and we obtain for zones I and III, respectively, 13.630 and 20.803 beads per mm^2. However, the number of attractive beads in each zone was not characterized. Zone III is more ordered than zone I since its histogram of the mutual distance is closer to a Rayleigh distribution around a length [cf. Fig. 7(b)] while the other is closer to a flat distribution without a feature length [see Fig. 7(e)]. Analogously, from this distribution we can compute the Shannon or information entropy S_e and obtain for each zone, respectively, $S_e(\mathrm{III}) = 0.00767$ and $S_e(\mathrm{I}) = 0.021$. Therefore, the evolution of the number of defects as a function of time changes depending on the different configurations of the glass beads.

To measure the exponents of the coarsening laws, we have considered the following fitting curve $N(t) = \beta t^{-\alpha} + N_\infty$. Table I summarizes our results for different observation zones of the liquid crystal layer under study. Different coarsening laws are obtained over different zones of the sample. However, from this table, we are not able to establish a correlation between the density of vortices, Shannon entropy, and spatial distributions with their coarsening exponents found experimentally. This is because of not only the spatial distribution of

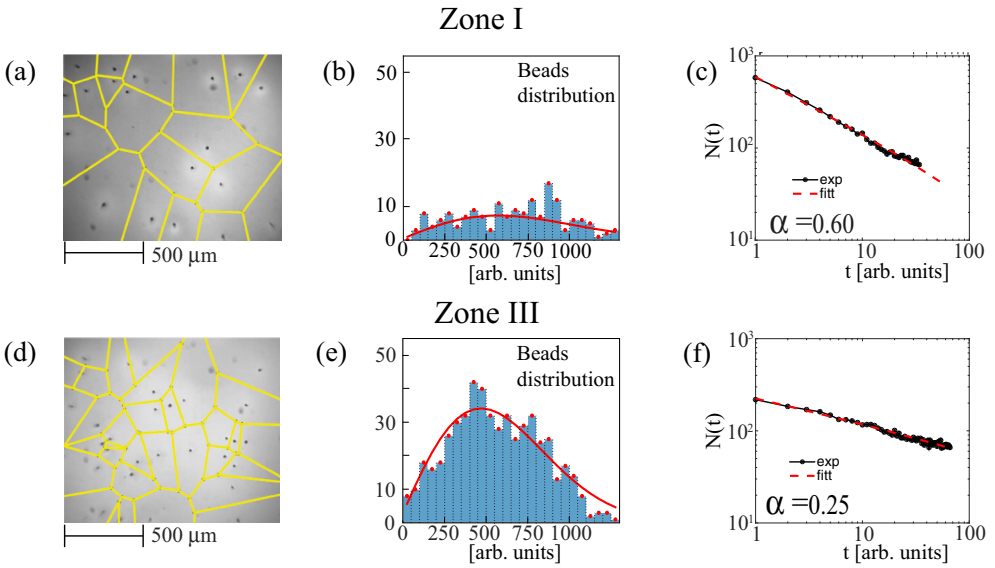

FIG. 7. Coarsening process of umbilical defects in an inhomogeneous sample analyzed over different observation zones, I and III. (a), (d) Voronoi diagram of glass beads in the observed zone, I and III, respectively. (b), (e) Histogram of the mutual distance of the glass beads. The solid curve is a fitting curve using a Rayleigh distribution. (c), (f) Corresponding scaling curves of the number of defects vs normalized time. Black points stand for the experimental data, dashed lines correspond to fitting curves of the form $N(t) = \beta/t^{\alpha} + N_{\infty}$ with $\alpha = 0.60$ and 0.25, respectively.

the glass beads matters but also how many of the glass beads are attractive or not. The effects due to the shape of the glass beads, and consequent vortex attraction, will be highlighted in the next section.

F. Defect dynamics in presence of a glass bead

The presence of the spherical spacers causes local deformation of the nematic director. Depending on their structure, the spacers can behave as localized potentials on the generated defects. Figure 8(a) shows a temporal sequence of snapshots of the vortex dynamics in the presence of a glass bead. Here, it is depicted the evolution of the umbilical defects under the influence of the bead. Figure 8(b) depicts the trajectories of the vortices. The dashed points (red) emphasize the positions of the vortices in different moments. In the temporal sequence, it is observed the temporal evolution of a pair of vortices with a positive and negative charge [cf. Fig. 8(b)]. Unexpectedly, both defects are attracted by the glass bead. From the trajectories, it appears clear that the vortex interaction is stronger than the vortex-bead interaction. Indeed, the vortices move close to the straight line that joins both vortices (see the dashed line in Fig. 8). However, close to the glass bead the trajectories are deflected and reoriented toward the center of the spacer. Finally, both vortices collide with the spacer and disappear. Hence, the observations show that the presence of inhomogeneities strongly affects the vortex dynamics and interactions.

To figure out the interaction between the vortices and the glass bead, we have repeated the experiment many times (∼50 experimental realizations) and monitored the collision of vortices, both with positive and negative charges, with the glass bead. This analysis is achieved by using circular crossed polarizers, which allows us distinguishing both topological charges with more precision. Figure 9 summarizes the different collision points between the vortices and the bead. The red (blue) points account for the collision points of positive

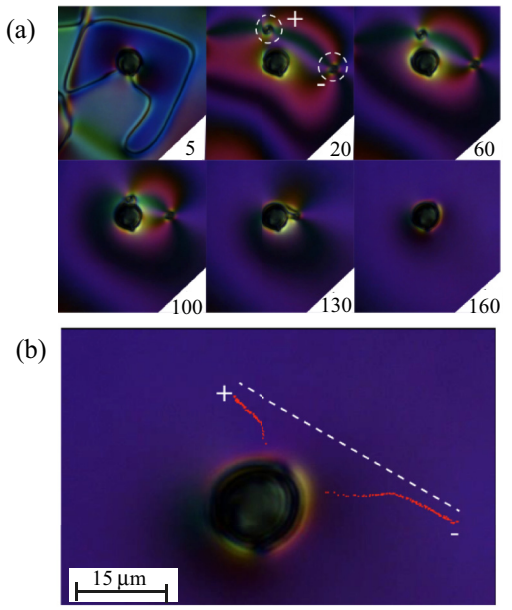

FIG. 8. Interaction between a glass bead and umbilical defects observed under linear crossed polarizers. (a) Sequences of temporal snapshots. The bottom numbers in each panel account for the respective frame. The temporal increment of each frame corresponds to 0.07 s. Umbilical defects of a positive (circular shape) and negative (square shape) charge under circular crossed polarizers are recognized and monitored. The dashed circles account for the umbilical defects. (b) Trajectory of the vortices: the dashed points (red) indicate the trajectory of defects, the dashed straight line accounts for the initial distance between defects.

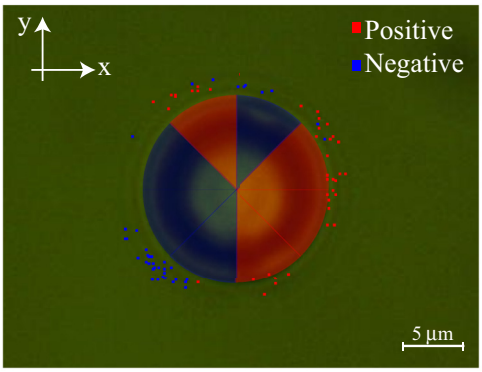

FIG. 9. Quadrupolar structure generated by a glass bead in the liquid crystal medium. Experimental characterization of the collision points of the umbilical defects for different experimental realizations. In most of the realizations only one defect collides with the bead. The dark (blue) and light (red) points account for the collision points of positive, respectively, negative vortices. The color areas highlight the different collision regions of the bead.

(negative) vortices. From this figure, it is possible to infer that the glass bead has a quadrupolar structure. Namely, the vortices of a given charge prefer to collide in certain parts of the bead. Note that the observed poles are not symmetric, which is a manifestation that dipolar terms are also relevant in the interactions. Experimentally, the vortex-bead interaction is weaker than the interaction between the umbilical defects. It is well known that glass beads without surface treatment generate homeotropic anchoring at their boundaries, that is, the liquid crystal molecules tend to be oriented normal to the surface of the glass bead [36,41]. In addition, due to the fact that the glass bead is in contact with the glass plates of the sample, one expects a Saturn-ring-like defect loop to appear around each glass inclusion [36,41]. Figure 10 shows a schematic representation of the director field lines induced by a perfect spherical glass bead and a slightly deformed bead. When the glass bead is perfectly spherical, it generates a defect in the center, which is canceled with the equivalent charge caused by the Saturn ring. In Fig. 10, the induced charge is represented by a central point (blue) and the Saturn ring by a closed curve (green). Therefore, perfectly spherical glass beads cause the net charge to cancel out, that is, the

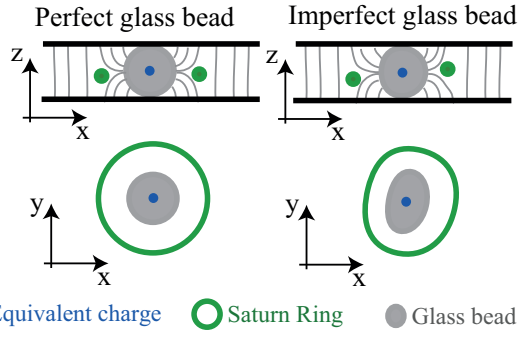

FIG. 10. Schematic representation of the director field lines induced by a perfect spherical bead (left panel) and a slightly deformed bead (right panel). Upper and lower panels show a side and top view of the correspondingly induced defects.

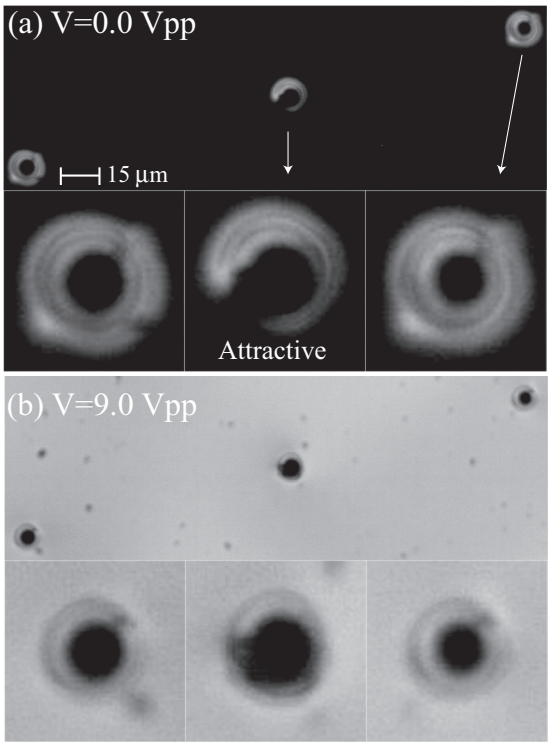

FIG. 11. Optical micrograph of active and passive glass beads. Snapshots of a liquid crystal sample within linear crossed polarizers without (top panel) and with (bottom panel) voltage. The lateral beads are passive, while the central bead is active.

equivalent charge of the Saturn ring coincides with the charge induced in the center. These glass beads are characterized by not attracting vortices so that we name them as *passive beads*. In contrast, deformed glass beads generate equivalent multipolar charges (dipoles, quadrupole, and so forth), which are neutral but affect the dynamics of their surroundings. In particular, these glass beads with multipolar charges are characterized by attracting and annihilating vortices and we name them *active beads*. Experimentally, these glass beads with multipolar charges can be detected since when no voltage is applied to the sample under cross polarizers, the perfect and imperfect glass beads generate perfect rings or deformed curves of light, respectively. Figure 11 shows three glass beads with and without voltage, in which one can identify the deformed glass bead (central). Only this central glass bead attracts vortices.

In brief, spherical glass beads do not attract or repel umbilical defects. On the other hand, when the glass beads are not perfect, the equivalent charge of the glass bead and that of the Saturn ring do not coincide, creating a multipolar charge for the interaction with the defects. Hence, the interaction of an imperfect glass bead and umbilical defect can be modeled by

$$M\dot{\mathbf{r}} = q\left[\frac{\vec{d}}{||\mathbf{r}||^2} - \frac{\vec{d}\cdot\mathbf{r}}{||\mathbf{r}||^4}\mathbf{r}\right] + q\left[\frac{\vec{l}^2}{||\mathbf{r}||^4}\mathbf{r} + \frac{2\vec{l}(\vec{l}\cdot\mathbf{r})}{||\mathbf{r}||^4}\right], \quad (10)$$

where $\mathbf{r}(\mathbf{t})$ is the vector that joins the position between the glass bead and the vortex, $||\mathbf{r}||$ is the magnitude of the vector $\mathbf{r}$, $\vec{d}$ is a vector that characterizes the dipolar interaction, q is

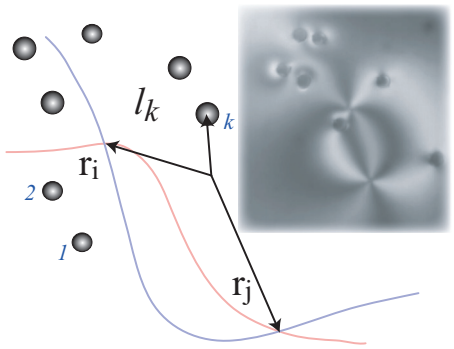

FIG. 12. Schematic representation of the vortex-pair interaction in the presence of glass beads. The index k accounts for the kth glass bead. $\mathbf{r_i}$ is the vector position of ith vortex. $\mathbf{l_k}$ is the vector position of the kth glass bead. The inset is an experimental snapshot obtained with the sample in-between crossed linear polarizers.

the topological charge of the interacting vortex, $\vec{l}$ is a vector that characterizes the quadrupolar interaction, and M stands for the vortex mobility. Note that the vectors $\vec{l}$ and $\vec{d}$ are not necessary parallels. On the right-hand side of Eq. (10), the first and second parentheses terms account, respectively, for the dipolar and quadrupolar interactions. Note that the dipolar and quadrupole interactions decay with the square and the cubic inverse of the distance between the vortices and the beads, respectively. From the experimental observations, we deduce that the quadrupole interaction is more dominant in the interaction ($\vec{d} \ll \vec{l}$, see Fig. 9). It is important to note that most of the glass beads do not attract vortices. However, the strength and direction parameters change each bead. Then, a detailed characterization of the vortex dynamics in a medium with spacers is a complex problem.

IV. SCREENING EFFECT AND COARSENING

The experimental observations show that some glass beads exert a force, either attractive or repulsive, on the vortices. Such a force is a power of the inverse of the distance between the bead and the vortices and has a different strength depending on the particular active bead considered. In order to shed light on the statistical vortex dynamics, let us consider two vortices in the presence of N' glass beads, as depicted in Fig. 12. For the sake of simplicity, we consider that glass beads are dominantly dipolar, *dipolar medium*.

Furthermore, we will use a similar strategy to derive third Kepler's law in the solar system, which is based on the fact that the n-body interaction (not self-similar) is approximated by the two-body interaction (self-similar), from which the third Kepler's law is inferred [42]. Let us consider a vortex gas in the presence of randomly distributed beads, which is described by

$$M\dot{\mathbf{r}}_\mathbf{i} = \sum_{j}^{N-1} \frac{q_{ij}}{||\mathbf{r_i}-\mathbf{r_j}||^2}(\mathbf{r_i}-\mathbf{r_j}) + \sum_{k=1}^{N'}\left[\frac{Q_{ik}\vec{d}_k}{||\mathbf{r_i}-\mathbf{l_k}||^2} - \frac{Q_{ik}[(\mathbf{r_i}-\mathbf{l_k})\cdot\vec{d}_k]}{||\mathbf{r_i}-\mathbf{l_k}||^4}(\mathbf{r_i}-\mathbf{l_k})\right], \quad (11)$$

where $\mathbf{r_i}$ stands for the position vector of ith vortex (cf. Fig. 12), M is the vortex mobility, q_{ij} is the product of the topological charges of the ith and jth vortices, Q_{ik} is the intensity of the interaction between the vortex, N and N' account for the number of vortices and beads and the kth bead, $\mathbf{l_k}$ and $\vec{d}_k$ are the vector position and the dipolar vector of kth glass bead, respectively.

Let us consider the limit of diluted vortices, that is, the distance between vortices $r \approx ||\mathbf{r_i}-\mathbf{r_j}||$ is much greater than the distance between a vortex and glass beads surrounding it ($||\mathbf{r_i}-\mathbf{r_j}| \gg ||\mathbf{r_i}-\mathbf{l_k}||$). Hence, the nearby glass beads dominate the dynamics of vortices, that is,

$$M\dot{\mathbf{r}}_\mathbf{i} \approx \sum_{k=1}^{N'} \frac{Q_{ik}}{||\mathbf{r_i}-\mathbf{l_k}||^2}\vec{d}_k + \sum_{k=1}^{N'} \frac{Q_{ik}(\mathbf{r_i}-\mathbf{l_k})\cdot\vec{d}_k}{||\mathbf{r_i}-\mathbf{l_k}||^4}(\mathbf{r_i}-\mathbf{l_k}). \quad (12)$$

In this limit, the dynamics of the vortices is not self-similar, however, when performing the transformation of spatial and temporal dilation

$$\mathbf{r_i} \to \lambda\mathbf{r_i}, \qquad t \to \lambda^3 t. \quad (13)$$

Eq. (15) takes the form

$$M\dot{\mathbf{r}}_\mathbf{i} \approx \sum_{k=1}^{N'} \frac{Q_{ik}\vec{d}_k}{||\mathbf{r_i}-\frac{\mathbf{l_k}}{\lambda}||^2} + \sum_{k=1}^{N'} \frac{Q_{ik}(\mathbf{r_i}-\frac{\mathbf{l_k}}{\lambda})\cdot\vec{d}_k}{||\mathbf{r_i}-\frac{\mathbf{l_k}}{\lambda}||^4}\left(\mathbf{r_i}-\frac{\mathbf{l_k}}{\lambda}\right). \quad (14)$$

The coarsening process is governed for large times and distances; therefore, one can consider λ to be large ($\lambda \gg 1$). Then, the above equation is rewritten

$$M\dot{\mathbf{r}}_\mathbf{i} \approx \sum_{k=1}^{N'} \frac{Q_{ik}\vec{d}_k}{||\mathbf{r_i}||^2} + \sum_{k=1}^{N'} Q_{ik}\frac{\mathbf{r_i}\cdot\vec{d}_k}{||\mathbf{r_i}||^4}\mathbf{r_i} + O\left(\frac{1}{\lambda}\right), \quad (15)$$

so that, if one dilates space and time on large scales, the equivalent set of Eqs. (5) are invariant at the dominant order. Furthermore, the vortex gas in such a disordered medium satisfies an effective dynamics governed by the previous interaction law. As we have mentioned before, the number of vortices at time t can be expressed as $N(t) = A/\langle r\rangle^2$, where A is the area of the sample under study and $\langle r\rangle$ is the average distance between vortices. Then, $\langle r\rangle$ and $N(t)$ should also be self-similar with the transformation (13). Hence, $N(\lambda^3 t) = A/\lambda^2\langle r\rangle^2$, and we obtain

$$N(t) = \frac{\beta_0}{t^{2/3}}, \quad (16)$$

where β_0 is constant. From this scaling law we obtain that the number of defects decreases with a $\alpha = -\frac{2}{3}$ power. Experimentally, several zones show exponents close to $-\frac{2}{3}$ (see Table I). Note that all the investigated zones, except zone III, show an exponent within 20% error from the $-\frac{2}{3}$ theoretical prediction. However, the dynamics of submerged vortices in an environment full of beads with various imperfections is much more complicated, as illustrated by the experimental results, and a full agreement over all the investigated zones could not be reached.

V. CONCLUSIONS AND REMARKS

Far from equilibrium systems with the coexistence of equilibria exhibit rich and complex defect dynamics in order to reach a more stable configuration. This dynamics of defects generates a rich variety of spatial textures. Defects in rotationally invariant two-dimensional systems attract a great deal of attention because of their universal character and intriguing topological properties. Nematic liquid crystals layer with negative dielectric constant and homeotropic anchoring under the influence of a voltage are the ideal context for studying the interaction of gas of topological vortices with opposite topological charges. One expects the dynamics of the vortices being characterized by a decreasing number in time, which follows a power law with critical exponent $\alpha = 1$ because the dominant interaction between the vortices is self-similar. Unexpectedly, we observe that this dynamics is persistent in thin cells of nematic liquid crystals that contain glass beads as spacers. However, the laws of the exponential decay in the number of vortices depend strongly on the distribution of the glass beads and their imperfections. Experimentally, we have characterized such a dynamics and demonstrated that the deformed glass beads attract vortices of opposite topological charges, presenting mainly a quadrupolar behavior. Theoretically, we have derived the modified power law for inhomogeneous samples, leading to $\alpha = \frac{2}{3}$ exponent of the power law. The agreement with the exponents derived from the experimental observations is satisfactory over several zones of the analyzed samples. However, a complete agreement could not be reached because of the diversity of the beads and the consequent complexity of the induced vortex dynamics.

Liquid crystal cells with spacers are fundamental in the development of displays of various electronic devices. The influence that the disperse beads, often used as spacers in the cell, can exert on the molecular reorientation is usually ignored. Our observations show that the inhomogeneities induced by the beads can play a relevant role in the dynamics of defects. Therefore, the study of the interaction between spacers and the surrounding liquid crystal can reveal important features of molecular behavior and could be taken into account for further improvements of liquid crystal devices.

ACKNOWLEDGMENTS

M.G.C. and V.Z. acknowledge financial support from the Millennium Institute for Research in Optics and FONDECYT Project No. 1180903.

[1] P. Ball, *The Self-Made Tapestry: Pattern Formation in Nature* (Oxford University Press, New York, 1999).
[2] P. Glansdorff and I. Prigogine, *Thermodynamic Theory of Structures, Stability and Fluctuations* (Wiley, New York, 1971).
[3] G. Nicolis and I. Prigogine, *Self-Organization in Non Equilibrium Systems* (Wiley, New York, 1977).
[4] M. C. Cross and P. C. Hohenberg, Rev. Mod. Phys. **65**, 851 (1993).
[5] L. M. Pismen, *Patterns and Interfaces in Dissipative Dynamics, Springer Series in Synergetics* (Springer, Berlin, 2006).
[6] M. Cross and H. Greenside, *Pattern Formation and Dynamics in Nonequilibrium Systems* (Cambridge University Press, New York, 2009).
[7] C. Kittel, *Introduction to Solid State Physics* (Wiley, New York, 1976).
[8] L. M. Pismen, *Vortices in Nonlinear Fields* (Clarendon, Oxford 1999).
[9] R. Barboza, U. Bortolozzo, G. Assanto, E. Vidal-Henriquez, M. G. Clerc, and S. Residori, Vortex Induction via Anisotropy Stabilized Light-Matter Interaction, Phys. Rev. Lett. **109**, 143901 (2012).
[10] R. Barboza, U. Bortolozzo, S. Residori, and E. Vidal-Henriquez, Optical vortex induction via light–matter interaction in liquid-crystal media, Adv. Opt. Photonics **7**, 635 (2015).
[11] E. Calisto, M. G. Clerc, M. Kowalczyk, and P. Smyrnelis, On the origin of the optical vortex lattices in an nematic liquid crystal light valve, Opt. Lett. **44**, 2947 (2019).
[12] S. Chandrasekhar, *Liquid Crystals* (Cambridge University Press, Cambridge 1992).
[13] P. G. de Gennes and J. Prost, *The Physics of Liquid Crystals*, 2nd ed. (Clarendon, Oxford, 1993).
[14] P. Oswald and P. Pieranski, *Nematic and Cholesteric Liquid Crystals* (Taylor & Francis, Boca Raton, FL, 2005)
[15] V. Freedericksz and V. Zolina, Forces causing the orientation of an anisotropic liquid, Trans. Faraday Soc. **29**, 919 (1927).
[16] A. Rapini, Umbilics: static properties and shear-induced displacements, J. Phys. (Paris) **34**, 629 (1973).
[17] O. Lehmann, Über fliessende krystalle, Z. Phys. Chem. **4U**, 462 (1889).
[18] G. Friedel, Les états mésomorphes de la matière Ann. Phys. (Paris) **18**, 273 (1922).
[19] F. C. Frank, Liquid crystals. On the theory of liquid crystals, Discuss. Faraday Soc. **25**, 19 (1958).
[20] T. Frisch, S. Rica, P. Coullet, and J. M. Gilli, Spiral Waves in Liquid Crystal, Phys. Rev. Lett. **72**, 1471 (1994).
[21] T. Frisch, Spiral waves in nematic and cholesteric liquid crystals, Phys. D (Amsterdam) **84**, 601 (1995).
[22] R. Barboza, T. Sauma, U. Bortolozzo, G., Assanto, M. G. Clerc, and S. Residori, Characterization of the vortex-pair interaction law and nonlinear mobility effects, New J. Phys. **15**, 013028 (2013).
[23] M. G. Clerc, E. Vidal-Henriquez, J. D. Davila, and M. Kowalczyk, Symmetry breaking of nematic umbilical defects through an amplitude equation, Phys. Rev. E **90**, 012507 (2014).
[24] E. Bodenschatz, W. Pesch, and L. Kramer, Structure and dynamics of dislocations in an anisotropic pattern-forming systems, Phys. D (Amsterdam) **32**, 135 (1988).
[25] F. Bethuel, H. Brezis, and F. Hélein, *Ginzburg-Landau Vortices* (Springer, New York, 2004).
[26] T. Nagaya, H. Hotta, H. Orihara, and Y. Ishibashi, Observation of annihilation process of disclinations emerging from bubble domains, J. Phys. Soc. Jpn. **60**, 1572 (1991).

[27] D. K. Ding and E. L. Thomas, Structures of point integer disclinations and their annihilation behavior in thermotropic liquid crystal polyesters, Mol. Cryst. Liq. Cryst. **241**, 103 (1994).

[28] I. Dierking, O. Marshall, J. Wright, and N. Bulleid, Annihilation dynamics of umbilical defects in nematic liquid crystals under applied electric fields, Phys. Rev. E **71**, 061709 (2005).

[29] A. N. Pargellis, S. Green, and B. Yurke, Planar XY-model dynamics in a nematic liquid crystal system, Phys. Rev. E **49**, 4250 (1994).

[30] M. Argentina, M. G. Clerc, R. Rojas, and E. Tirapegui, Coarsening dynamics of the one-dimensional Cahn-Hilliard model, Phys. Rev. E **71**, 046210 (2005).

[31] M. G. Clerc, S. Coulibaly, L. Gordillo, N. Mujica, and R. Navarro, Coalescence cascade of dissipative solitons in parametrically driven systems, Phys. Rev. E **84**, 036205 (2011).

[32] L. Ratke and P. W. Voorhees, *Growth and Coarsening: Ostwald Ripening in Material Processing* (Springer, New York, 2013).

[33] S. Hilgenfeldt, S. A. Koehler, and H. A. Stone, Dynamics of Coarsening Foams: Accelerated and Self-Limiting Drainage, Phys. Rev. Lett. **86**, 4704 (2001).

[34] T. Nagaya, H. Orihara, and Y. Ishibashi, Coarsening dynamics of +1 and -1 disclinations in two-dimensionally aligned nematics? Spatial distribution of disclinations, J. Phys. Soc. Jpn. **64**, 78 (1995).

[35] R. Barboza, U. Bortolozzo, M. G. Clerc, S. Residori, and V. Zambra, Coarsening dynamics of umbilical defects in inhomogeneous medium, in *Nonlinear Dynamics: Materials, Theory and Experiments* (Springer, Cham, 2016), pp. 31–43.

[36] K. Takatoh, M. Sakamoto, R. Hasegawa, M. Koden, N. Itoh, and M Hasegawa, *Alignment Technology and Applications of Liquid Crystal Devices* (CRC Press, Boca Raton, 2005), pp. 7–54.

[37] A. Gerrard and J. M. Burch, *Introduction to Matrix Methods in Optics* (Dover, New York, 1975).

[38] R. B. Meyer, On the existence of even indexed disclinations in nematic liquid crystals, Philos. Mag. **27**, 405 (1973).

[39] I. Dierking, Anisotropy in the annihilation dynamics of umbilic defects in nematic liquid crystals, Phys. Rev. E **85**, 021703 (2012).

[40] A. Okabe, N. Boots, K. Sugihara, and S. N. Chiu, *Spatial Tessellations: Concepts and Applications of Voronoi Diagrams* (Wiley, Chichester, 2009).

[41] H. Stark, Director field configurations around a spherical particle in a nematic liquid crystal, Eur. Phys. J. B **10**, 311 (1999).

[42] L. D. Landau and E. M. Lifshiftz, *Mechanics* (Pergamon, Oxford, 1976).